Technical note: In situ photosynthesis-irradiance curve determination in peatlands with a modulated-light skirt-chamber

Frederic Thalasso[1,2,*], Julio A. Salas-Rabaza[2,*], Brenda Riquelme del Río[2], Jorge F. Perez-Quezada[2,3,4], Cristian Gajardo[3], Matías Troncoso-Villar[2]

[1]Departamento de Biotecnología y Bioingeniería, Centro de Investigación y de Estudios Avanzados del Instituto Politécnico Nacional (Cinvestav), Av. IPN 2508, Mexico City 07360, Mexico
[2]Cape Horn International Center, Universidad de Magallanes, O'Higgins 310, Puerto Williams, Chile
[3]Department of Environmental Sciences and Renewable Natural Resources, University of Chile, Av. Santa Rosa 11315, La Pintana, Santiago, Chile
[4]Institute of Ecology and Biodiversity, Barrio Universitario Concepción, Chile

Correspondence to: Frederic Thalasso (thalasso@cinvestav.mx), Julio A. Salas-Rabaza (jsalasrab@gmail.com).

Supplementary Information

S1. Chamber design and mass balance

The new modulated-light skirt-chamber was manufactured using 3D printing with thermoplastic polyurethane and consists of two sections (Figure 1). The first section is a ring-shaped base with an outer diameter of 320 mm and an inner diameter of 240 mm. This base is designed to be placed on the ground, with the plastic skirt glued to its upper surface. The base can also accommodate a steel chain placed above the plastic skirt to improve sealing with the ground. Along the inner perimeter of the base, a 5×5 mm groove allows the chamber (second section) to be positioned hermetically using silicone grease for sealing. The chamber is an oblique cylinder cut at a 40° angle from the horizontal, with a minimum height of 40 mm, a maximum height of 250 mm, an internal diameter of 240 mm, and a thickness of 15 mm. This design, combined with its orientability, enhances direct sunlight exposure for most of the day, even at relatively high latitudes where sun inclination is low. The internal surface of the chamber is covered with a reflective film (Q-BICS, Mexico) to ensure maximum light dispersion. Around the oblique cut, a 10×10 mm support ledge runs along the entire perimeter, positioned just 10 mm below the cut edge, to support an oval window made of 9 mm-thick commercial glass window, which is sealed with silicone. Within the chamber, two light/temperature data loggers are placed at ground level to measure light intensity. On the higher side of the chamber, a 180×40 mm opening leads to a rectangular extension housing a battery-operated fan, facilitating air circulation within the chamber. This design prevents the creation of shadows from the electric fan and optimizes light distribution over the entire ground surface. Inlet and outlet ports, positioned on opposite sides of the frame, are connected in recirculation mode to an UGGA (Los Gatos Inc., ABB, USA), which continuously measures CH_4 and CO_2 concentrations at 1 Hz. In this study, we focus solely on CO_2 emissions, although CH_4 concentrations are measured when used as a tracer gas to determine the gas residence time within the chamber, as described in section 2.2.

The concept of the chamber is the absence of a collar penetrating the ground, thus minimizing disturbance and reducing deployment time, but leading to imperfect sealing at the ground-chamber

interface, allowing for gas exchange between the atmosphere and the chamber. Under these conditions, the mass balance of the chamber is as follows:

$$\frac{dC_{C,CO2}}{dt} = CO_2\ flux\ + input\ caused\ by\ leaks - output\ caused\ by\ leaks \quad \text{(S1)}$$

$$\frac{dC_{C,CO2}}{dt} = F_{CO2} \cdot \frac{A_C}{V_C} + \frac{Q_L}{V_C} \cdot C_{L,CO2} - \frac{Q_L}{V_C} \cdot C_{C,CO2} \quad \text{(S2)}$$

where $C_{C,CO2}$ is the CO_2 concentration within the chamber (µmol m^{-3}), F_{CO2} is the CO_2 flux captured by the chamber (µmol m^{-2} s^{-1}), A_C is the area of the chamber in contact with the ground (m^2), V_C is the chamber volume (m^{-3}), Q_L is the leak flow rate to/from the chamber (m^3 s^{-1}), and $C_{L,CO2}$ is the CO_2 concentration at ground level outside the chamber, entering with the leaks (µmol m^{-3}).

Given that Q_L/V_C is the dilution rate caused by leaks and is the inverse of the gas residence time within the chamber (θ_C, s), Equation S2 can be rewritten as follows:

$$\frac{dC_{CO2}}{dt} = F_{CO2} \cdot \frac{A_C}{V_C} + \frac{Q_L}{V_C} \cdot \left(C_{L,CO2} - C_{C,CO2}\right) = F_{CO2} \cdot \frac{A_C}{V_C} + \frac{\left(C_{L,CO2} - C_{C,CO2}\right)}{\theta_C} \quad \text{(S3; 1)}$$

In addition to Equation S3, like most gas analyzers, the UGGA includes a cavity where the gas pumped out from the chamber is measured, causing measurement delays. This introduces a slight difference between the gas concentration measured by the analyzer and the actual concentration within the chamber. To solve that aspect, the mass balance of the analyzer's cavity can be described as follows:

$$\frac{dC_{D,CO2}}{dt} = \frac{Q_D}{V_D} \cdot C_{C,CO2} - \frac{Q_D}{V_D} \cdot C_{D,CO2} = \frac{\left(C_{C,CO2} - C_{D,CO2}\right)}{\theta_D} \quad \text{(S4)}$$

where $C_{D,CO2}$ is the CO_2 concentration measured (within the detector; µmol m^{-3}), Q_D is the flow rate to/from the detector (m^3 s^{-1}), V_D is the detector's cavity volume (m^3), and θ_D is the gas residence time within the detector's cavity.

Equation S4 can be rewritten to obtain the actual CO_2 concentration, as follows:

$$C_{C,CO2} = \frac{dC_{D,CO2}}{dt} \cdot \theta_D + C_{D,CO2} \quad \text{(S5)}$$

By combining Equations S3 and S5, we obtain:

$$F_{CO2} = \left(\frac{dC_{C,CO2}}{dt} - \frac{\left(C_{L,CO2} - C_{C,CO2}\right)}{\theta_C}\right) \cdot \frac{V_C}{A_C} \quad \text{(S6)}$$

In which $C_{C,CO2}$ is replaced by Equation S5.

S2. Determination of the chamber residence time (θ_C)

Resolving Equation S6 requires the determination of θ_C. The strategy included the creation of a transient state of the gas concentration, using CH_4 as a tracer gas. CH_4 was chosen, because it is detected by the UGGA and does not interfere with F_{CO2} measurements. Thus, the transient state and the determination of θ_C can be done during flux measurement. In practice, a pulse of CH_4 was injected into the chamber. After the CH_4 pulse injection, the CH_4 concentration within the chamber ($C_{C,CH4}$) is artificially increased and then tends to decrease back to a steady-state concentration at which the chamber is under equilibrium with the environment. This transient decrease of $C_{C,CH4}$ at any time, can be described by the following mass balance (similar to Equation S1,2):

$$\frac{dC_{C,CH4}}{dt} = CH_4\ flux\ + input\ caused\ by\ leaks - output\ caused\ by\ leaks \quad \text{(S7)}$$

$$\frac{dC_{C,CH4}}{dt} = F_{CH4} \cdot \frac{A_C}{V_C} + \frac{Q_L}{V_C} \cdot \left(C_{L,CH4} - C_{C,CH4}\right) = F_{CH4} \cdot \frac{A_C}{V_C} + \frac{\left(C_{L,CH4} - C_{C,CH4}\right)}{\theta_C} \quad \text{(S8)}$$

In Equations S7 and S8 the variables are defined as follows: $C_{C,CH4}$ represents the CH_4 concentration inside the chamber (µmol m^{-3}); F_{CH4} denotes the CH_4 flux from the ecosystem (µmol m^{-2} s^{-1}); A_C represents the area of the chamber in contact with the ground (m^2); V_C represents the chamber volume (m^3); Q_L indicates the flowrate of gas exchange between the chamber and the exterior due to leaks (m^3 s^{-1}); and $C_{L,CH4}$ signifies the gas concentration at ground level outside the chamber (to be considered for leaks; µmol m^{-3}). The term Q_L/V_C is the dilution rate caused by the gas exchange between the chamber and the environment due to leak, which is the inverse of the mean residence time of the chamber (θ_C).

Under steady state, *i.e.* gas concentration not changing over time, Equation S8 would become:

$$0 = F_{CH4} \cdot \frac{A_C}{V_C} + \frac{\left(C_{L,CH4} - C^*_{C,CH4}\right)}{\theta_C} \quad \text{(S9)}$$

Where $C^*_{C,CH4}$ is the concentration within the chamber that would be observed under steady state, i.e. constant. Under these conditions, Equation S9 can be reorganized as:

$$F_{CH4} \cdot \frac{A_C}{V_C} = -\frac{\left(C_{L,CH4} - C^*_{C,CH4}\right)}{\theta_C} \quad \text{(S10)}$$

By combining Equations S8 and S10, we can write:

$$\frac{dC_{C,CH4}}{dt} = \frac{\left(C_{L.CH4} - C_{C,CH4}\right)}{\theta_C} - \frac{\left(C_{L.CH4} - C^*_{C,CH4}\right)}{\theta_C} = \frac{C^*_{C,CH4} - C_{C,CH4}}{\theta_C} \quad \text{(S11)}$$

By variable separation and integration S11 can be written:

$$\int_0^t \frac{d\left(C^*_{C,CH4} - C_{C,CH4}\right)}{\left(C^*_{C,CH4} - C_{C,CH4}\right)} = -\int_0^t \frac{dt}{\theta_C} \quad \text{(S12)}$$

$$ln \frac{\left(C^*_{C,CH4} - C_{C,CH4}\right)_t}{\left(C^*_{C,CH4} - C_{C,CH4}\right)_0} = -t/\theta_C \quad \text{(S13)}$$

$$\frac{C^*_{C,CH4} - C_{C,CH4,t}}{C^*_{C,CH4} - C_{C,CH4,0}} = e^{-t/\theta_C} \quad \text{(S14)}$$

And finally:

$$C_{C,CH4}(t) = C^*_{C,CH4} - (C^*_{C,CH4} - C_{C,CH4,0}) \cdot e^{-t/\theta_C} \quad \text{(S15)}$$

It is important to note that for θ_C determination, any section of $C_{C,CH4}$ is valid, regardless of the initial and final $C_{C,CH4}$ values. A corollary of this is that the mass of CH_4 injected into the chamber is unimportant, as long as it is detectable. The selected section of $C_{C,CH4}$ was used to calibrate Equation S14, with θ_C and $C_{SS,CH4}$ as adjustment parameters and through the minimization of the Root Mean Square Error.

S3. Determination of the detector's cavity residence time (θ_D)

For the determination of θ_D, the same strategy and Equation S14 were used, except that θ_D substitutes θ_C and that a step increase of $C_{C,CH4}$ at the detector inflow was used (no chamber) instead of a pulse concentration. Also, this determination was conducted in the laboratory, as θ_D is a detector parameter not changing over time.

Table S1: Percentage of light transmittance for the different fabrics used, as measured in the field under natural light conditions. Of the 11 fabrics tested, we progressively selected 6 that provided reliable data, which are marked with an asterisk.

Fabric	% transmittance	SD
None *	100.0%	-
1	85.2%	12.3%
2	57.4%	21.9%
3 *	51.1%	19.2%
4 *	35.9%	13.4%
5 *	22.3%	2.3%
6	21.2%	10.7%
7 *	15.5%	3.2%
8	12.7%	5.8%
9	5.0%	1.7%
10	1.1%	0.1%
11 *	0.4%	0.1%

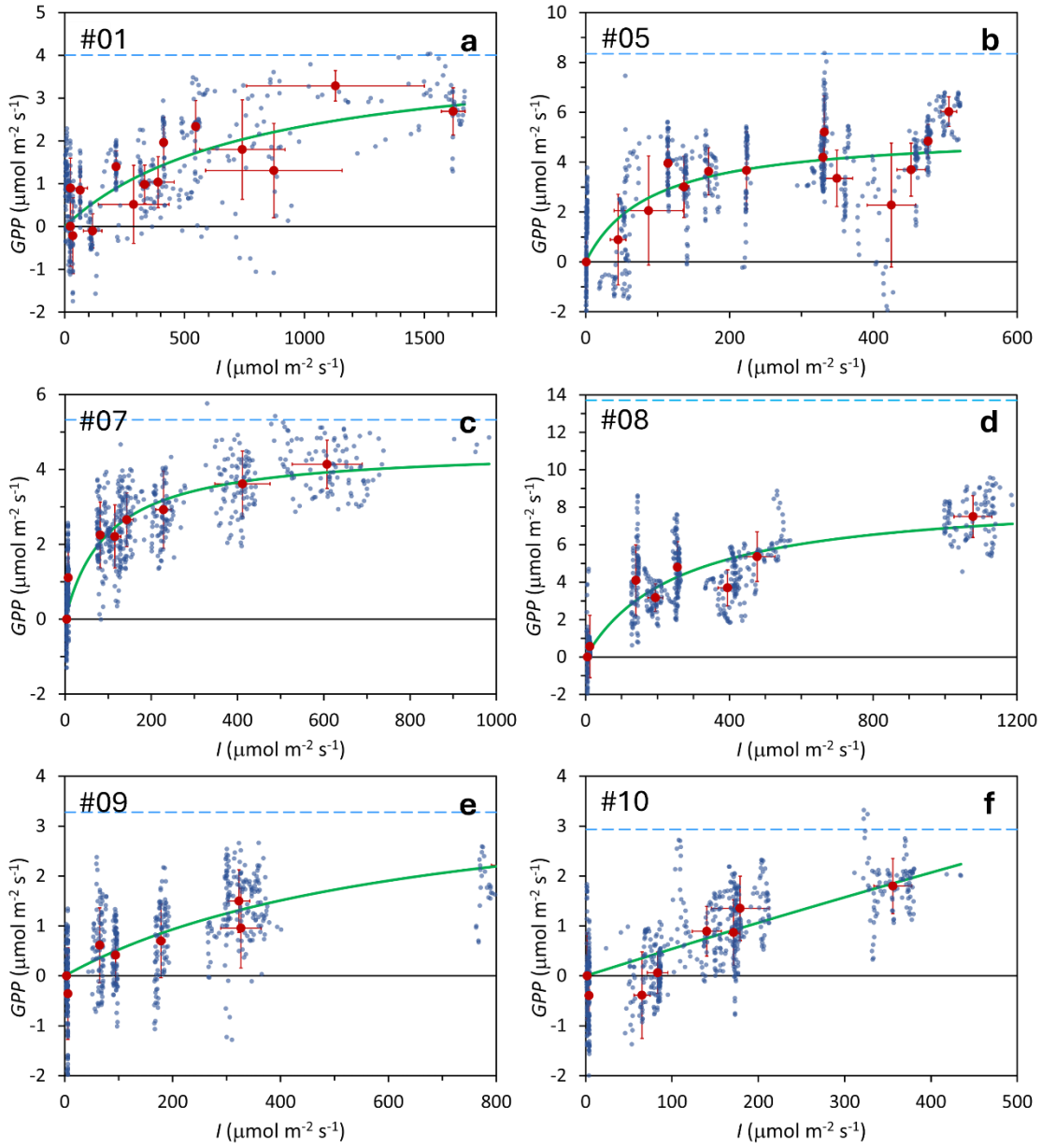

Figure S1 (1/2): Photosynthesis-Irradiance (PI) curves observed at 20 locations in a subantarctic peatland bog, measured *in situ* using the modulated-light skirt-chamber. Blue points represent individual measurements, with 500-900 data points collected at each location. Red points indicate the mean of data clusters collected under each irradiance level, corresponding to each screen of fabric used. Error bars on the red points represent one standard deviation. The green continuous lines represent the best fitting of the Monod model, and the red continuous line represents the best fitting of the Bernard-Rémond model. The light blue dashed line indicates the level of respiration, expressed in the same units as the *GPP*. The numbers indicated in the upper left corner reference the experiment numbers listed in Table 1, where model parameters and statistics are provided.

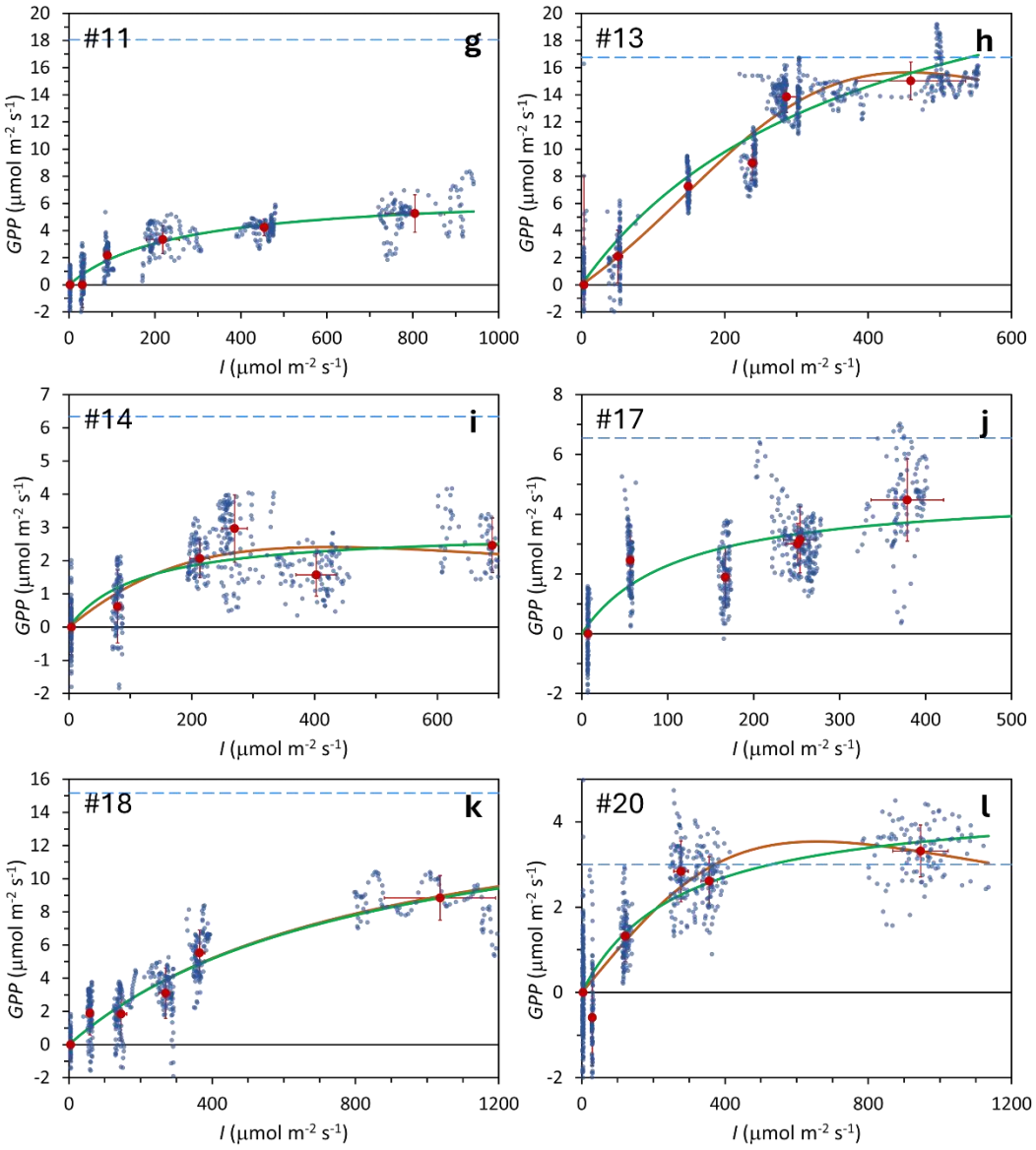

Figure S1 (2/2): Photosynthesis-Irradiance (PI) curves observed at 20 locations in a subantarctic peatland bog, measured *in situ* using the modulated-light skirt-chamber. Blue points represent individual measurements, with 500-900 data points collected at each location. Red points indicate the mean of data clusters collected under each irradiance level, corresponding to each screen of fabric used. Error bars on the red points represent one standard deviation. The green continuous lines represent the best fitting of the Monod model, and the red continuous line represents the best fitting of the Bernard-Rémond model. The light blue dashed line indicates the level of respiration, expressed in the same units as the *GPP*. The numbers indicated in the upper left corner reference the experiment numbers listed in Table 1, where model parameters and statistics are provided.

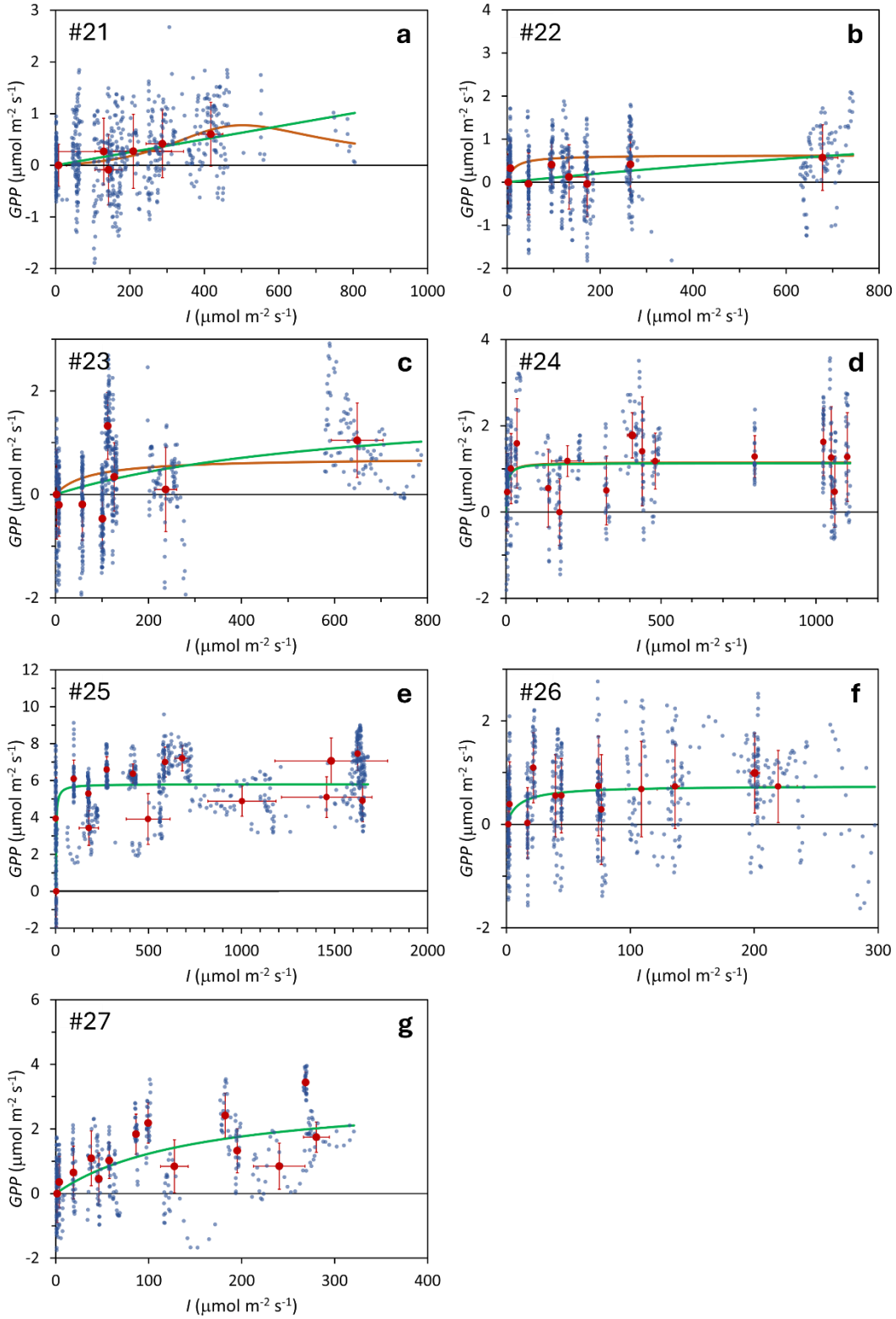

Figure S2: Photosynthesis-Irradiance (PI) curves that were rejected due to failed fitting of the Monod and Bernard-Rémond models.